

Opto-Electronic Science

ISSN 2097-0382

CN 51-1800/O4

Robust measurement of orbital angular momentum of a partially coherent vortex beam under amplitude and phase perturbations

Zhao Zhang, Gaoyuan Li, Yonglei Liu, Haiyun Wang, Bernhard J. Hoenders, Chunhao Liang, Yangjian Cai and Jun Zeng

Citation: Zhang Z, Li GY, Liu YL, et al. Robust measurement of orbital angular momentum of a partially coherent vortex beam under amplitude and phase perturbations. *Opto-Electron Sci* **3**, 240001 (2024).

<https://doi.org/10.29026/oes.2024.240001>

Received: 19 September 2023; Accepted: 5 January 2024; Published online: 31 January 2024

Related articles

Robust far-field imaging by spatial coherence engineering

Yonglei Liu, Yahong Chen, Fei Wang, Yangjian Cai, Chunhao Liang, Olga Korotkova
Opto-Electronic Advances 2021 **4**, 210027 doi: [10.29026/oea.2021.210027](https://doi.org/10.29026/oea.2021.210027)

Measurement of optical coherence structures of random optical fields using generalized Arago spot experiment

Xin Liu, Qian Chen, Jun Zeng, Yangjian Cai, Chunhao Liang
Opto-Electronic Science 2023 **2**, 220024 doi: [10.29026/oes.2023.220024](https://doi.org/10.29026/oes.2023.220024)

Tailoring spatiotemporal dynamics of plasmonic vortices

Xinyao Yuan, Quan Xu, Yuanhao Lang, Xiaohan Jiang, Yuehong Xu, Xieyu Chen, Jie Han, Xueqian Zhang, Jiaguang Han, Weili Zhang
Opto-Electronic Advances 2023 **6**, 220133 doi: [10.29026/oea.2023.220133](https://doi.org/10.29026/oea.2023.220133)

100 Hertz frame-rate switching three-dimensional orbital angular momentum multiplexing holography via cross convolution

Weijia Meng, Yilin Hua, Ke Cheng, Baoli Li, Tingting Liu, Qinyu Chen, Haitao Luan, Min Gu, Xinyuan Fang
Opto-Electronic Science 2022 **1**, 220004 doi: [10.29026/oes.2022.220004](https://doi.org/10.29026/oes.2022.220004)

More related article in Opto-Electronic Journals Group website 



Opto-Electronic
Science

<http://www.ojournal.org/oes>



 OE_Journal



Website

DOI: [10.29026/oes.2024.240001](https://doi.org/10.29026/oes.2024.240001)

Robust measurement of orbital angular momentum of a partially coherent vortex beam under amplitude and phase perturbations

Zhao Zhang^{1,2}, Gaoyuan Li¹, Yonglei Liu³, Haiyun Wang⁴,
Bernhard J. Hoenders⁵, Chunhao Liang^{1,2,6*}, Yangjian Cai^{1,2,6*} and
Jun Zeng^{1,2,6*}

The ability to overcome the negative effects, induced by obstacles and turbulent atmosphere, is a core challenge of long-distance information transmission, and it is of great significance in free-space optical communication. The spatial-coherence structure, that characterizes partially coherent fields, provides a new degree of freedom for carrying information. However, due to the influence of the complex transmission environment, the spatial-coherence structure is severely damaged during the propagation path, which undoubtedly limits its ability to transmit information. Here, we realize the robust far-field orbital angular momentum (OAM) transmission and detection by modulating the spatial-coherence structure of a partially coherent vortex beam with the help of the cross-phase. The cross-phase enables the OAM information, quantified by the topological charge, hidden in the spatial-coherence structure can be stably transmitted to the far field and can resist the influence of obstructions and turbulence within the communication link. This is due to the self-reconstruction property of the spatial-coherence structure embedded with the cross-phase. We demonstrate experimentally that the topological charge information can be recognized well by measuring the spatial-coherence structure in the far field, exhibiting a set of distinct and separated dark rings even under amplitude and phase perturbations. Our findings open a door for robust optical signal transmission through the complex environment and may find application in optical communication through a turbulent atmosphere.

Keywords: degree of coherence; orbital angular momentum; cross-phase; topological charge; information transmission

Zhang Z, Li GY, Liu YL et al. Robust measurement of orbital angular momentum of a partially coherent vortex beam under amplitude and phase perturbations. *Opto-Electron Sci* **3**, 240001 (2024).

Introduction

The beam with spiral phase, described by $\exp(i\ell\theta)$, is re-

ferred to as the vortex beam¹. Each photon of the vortex

beam carries an orbital angular momentum (OAM) of $\ell\hbar$,

¹Shandong Provincial Engineering and Technical Center of Light Manipulations & Shandong Provincial Key Laboratory of Optics and Photonic Device, School of Physics and Electronics, Shandong Normal University, Jinan 250358, China; ²Collaborative Innovation Center of Light Manipulation and Applications, Shandong Normal University, Jinan 250358, China; ³School of Physical Science and Technology, Soochow University, Suzhou 215006, China; ⁴School of Physical Science and Technology, Suzhou University of Science and Technology, Suzhou 215009, China; ⁵Zernike Institute for Advanced Materials, University of Groningen, Nijenborgh 4, NL-9747 AG Groningen, The Netherlands; ⁶Joint Research Center of Light Manipulation Science and Photonic Integrated Chip of East China Normal University and Shandong Normal University, East China Normal University, Shanghai 200241, China.

*Correspondence: CH Liang, E-mail: chunhaoliang@sndu.edu.cn; YJ Cai, E-mail: yangjian_cai@163.com; J Zeng, E-mail: zengjun@sndu.edu.cn
Received: 19 September 2023; Accepted: 5 January 2024; Published online: 31 January 2024



Open Access This article is licensed under a Creative Commons Attribution 4.0 International License.

To view a copy of this license, visit <http://creativecommons.org/licenses/by/4.0/>.

© The Author(s) 2024. Published by Institute of Optics and Electronics, Chinese Academy of Sciences.

where l is the topological charge, θ is the azimuthal angle, and \hbar is the reduced Planck constant. These modes provide a (theoretically) infinite and easily realized alphabet for encoding information and have been used extensively in optical communication². Due to carrying a discrete topological charge and its close relation with OAM, the interest in vortex beam has been rising and has yielded a lot in other applications, including optical trapping³⁻⁵, optical imaging⁶⁻⁷, optical measurement⁸, optical coding⁹, quantum information processing¹⁰ and holography¹¹.

Most studies on vortex beams have been restricted to fully coherent optical fields, which are easily affected by perturbing obstacles, such as aerosols, and a turbulent atmosphere. These perturbations introduce scintillation, distortion in the topological structure, and crosstalk between OAM modes, thereby limiting the performance of information transmission¹²⁻¹⁴. It has been well recognized that a partially coherent light beam, obtained by reducing the spatial coherence, can be able to resist the distortion induced by the obstacles mentioned above, and improve the effectiveness of information transfer in a communication channel with obstacles and a turbulent atmosphere^{15,16}. On the other hand, it has been shown that the spatial-coherence structure (i.e., degree of coherence) of the partially coherent beam can be viewed as an efficient degree of freedom to govern its propagation properties¹⁷ and its ability to transmit/carry information¹⁸. The combination of coherence and vortex phase has proven to be of advantage in free-space optical communication¹⁹, optical anti-counterfeiting²⁰, anti-noise optical imaging²¹ and versatility optical trapping^{22,23}.

The topological properties of vortex optical fields play an important role in the development of practical applications. If beams possessing both partial coherence and vortex structures are to be used effectively, it is of great significance to be able to properly characterize the TC of a partially coherent vortex beam. However, the traditional schemes for detecting OAM or topological charge²⁴, such as mode converters, interferometers, diffraction and Fourier analysis, are only limited to fully coherent vortex light and fail when the coherence decreases²⁵. To overcome this limitation, methods based on measuring the spatial-coherence structure have been proposed, but they are all only applicable for measurements under conditions without obstacle perturbation²⁶⁻²⁹, which excludes measurements in a complex transmission environ-

ment. Although Liu *et al.* demonstrated that the spatial-coherence structure exhibits a certain anti-disturbance property, but their research only restricted to non-vortex partially coherent light fields³⁰⁻³¹. Liu and Peng studied the evolution of the vortex light field and found that the ring-shaped coherent structure induced by the vortex phase was severely damaged by the obstacles³²⁻³³, making it difficult to extract accurate topological charge information from its far-field coherent structure. Therefore, the conclusion for the non-vortex beams does not directly extend to the vortex beams. This is because the complex effect of obstacles and the turbulent atmosphere on the vortex phase, results in the chaotic splitting and the destruction of the spatial-coherence structure^{32,33}, the annihilation and generation of coherent vortices^{34,35} and beam random scintillation³⁶, which seriously hinders the accurate detection of the topological charge. Thus, measurement of the topological charge based on modulation of the spatial-coherence structure of a partially coherent vortex beams in complex transmission environment is still challenging.

Over the past few years, a new type of twisting phase known as the cross-phase has been explored by various research groups³⁷⁻⁴⁰. The cross phase is a quadratic phase structure distinct from the ordinary twist phase⁴¹, which finds versatile applications in coherent modes conversion³⁷, beam rotation³⁸, and optical vortices manipulation³⁹, and flexible beam focus⁴⁰. More recently, cross phase has been used to enhance the anti-disturbance ability of light beams during transmission, but so far has been limited to non-vortex circumstances^{30,31}. In this work, we find that by introducing the cross-phase into the degree of coherence structure of a partially coherent vortex beam, the far-field spatial-coherence structure can remain invariant even with an obstacle and a turbulent in propagation channels. Thus, the topological charge information encoded in the spatial-coherence structure can be robustly transmitted to the far field. This finding is demonstrated through numerical examples and experiment. Further, based on the peculiar self-reconstruction property of the degree of coherence, an efficient approach is proposed for detecting topological charge under amplitude and phase perturbations. Indeed, the obtained topological charge information in the degree of coherence structure is shown to be resistant to the negative effects induced by obstacles and atmospheric turbulence. This coherence-based technique greatly improves the ability to measure the topological properties of

partially coherent vortex beams.

This paper is organized as follows: Firstly, the theoretical model and computational propagation model for a partially coherent Laguerre Gaussian (PCLG) beam under amplitude and phase perturbation are given. Secondly, the effect of the cross-phase on the far-field degree of coherence of a PCLG beam is presented theoretically and principally. Thirdly, the robust transport and determination of the topological charge of a PCLG beam with a cross-phase under amplitude perturbation and phase perturbation are studied theoretically. Fourthly, the experiment is carried out to demonstrate the robust transport of the degree of coherence under amplitude perturbation and phase perturbation, and the robust identification of the topological charge based on measuring the degree of coherence is demonstrated. At last, the results are then summarized in Section *Conclusions*.

Theoretical model for a PCLG beam and computational propagation model for a PCLG beam under amplitude and phase perturbations

In the space-frequency domain, the second-order statistical properties of partially coherent sources, propagating along the z -axis, can be described in terms of their cross-spectral density function. In the source plane ($z = 0$), the cross-spectral density function of a partially coherent beam carrying a cross-phase has the following form³⁰:

$$W(\mathbf{r}_1, \mathbf{r}_2) = \tau_0(\mathbf{r}_1) \tau_0^*(\mathbf{r}_2) \mu(\Delta\mathbf{r}) \exp[iu(r_{1x}r_{1y} - r_{2x}r_{2y})], \quad (1)$$

where $\mathbf{r}_i = (r_{ix}, r_{iy})$ ($i=1, 2$) denotes the radial coordinates. $\tau_0(\mathbf{r})$ denotes a complex function, defined below. $\Delta\mathbf{r} = \mathbf{r}_1 - \mathbf{r}_2$ is the difference of two position vectors and $\mu(\Delta\mathbf{r})$ denotes the degree of coherence function of a partially coherent beam. The last term $\exp[iu(r_{1x}r_{1y} - r_{2x}r_{2y})]$ is the cross-phase structure, where the quantity u is a measure of the strength of the cross-phase and its sign property (positive or negative value) is only used to determine the rotation direction of the beam³⁸. For mathematical convenience and practicality of the conclusions, we consider using the PCLG beam, which is the most widely used and easily generated in the laboratory, as the source beam. In this case, the terms $\tau_0(\mathbf{r})$ and $\mu(\Delta\mathbf{r})$ are given as follows:

$$\tau_0(\mathbf{r}) = \left(\frac{\sqrt{2}\mathbf{r}}{\omega}\right)^l \exp\left(-\frac{\mathbf{r}^2}{\omega^2}\right) \exp(i l \varphi), \quad (2)$$

and

$$\mu(\Delta\mathbf{r}) = \exp\left[-\frac{(\Delta\mathbf{r})^2}{2\sigma^2}\right], \quad (3)$$

respectively. φ denotes the azimuthal (angle) coordinates. The quantity l refers to the topological charge¹. ω and σ denote the transverse beam width and transverse coherence width, respectively.

In some practical situations, the beam will be affected by amplitude perturbation and phase perturbation, which will greatly limit its application capabilities. To study the propagation characteristics of partially coherent beams under amplitude perturbation, we assume here that an opaque obstacle with center occlusion angle α is put in the source plane. The beam is obstructed by this obstacle and then propagates to the receiver plane. Within the accuracy of the paraxial approximation, the propagation of a PCLG beam, partially blocked by a sector-shaped opaque obstacle passing through an ABCD optical system, can be studied with the help of the generalized Collins integral^{32,42}:

$$\begin{aligned} W(\boldsymbol{\rho}_1, \boldsymbol{\rho}_2) &= \frac{1}{(\lambda B)^2} \exp\left[-\frac{ikD}{2B}(\boldsymbol{\rho}_1^2 - \boldsymbol{\rho}_2^2)\right] \\ &\times \int_0^\infty \int_0^\infty \int_{\alpha/2}^{2\pi-\alpha/2} \int_{\alpha/2}^{2\pi-\alpha/2} W(\mathbf{r}_1, \mathbf{r}_2) \\ &\times \exp\left[-\frac{ikA}{2B}(\mathbf{r}_1^2 - \mathbf{r}_2^2)\right] \\ &\times \exp\left\{\frac{ik}{B}[\mathbf{r}_1 \boldsymbol{\rho}_1 \cos(\theta_1 - \varphi_1) - \mathbf{r}_2 \boldsymbol{\rho}_2 \cos(\theta_2 - \varphi_2)]\right\} \\ &\times \mathbf{r}_1 \mathbf{r}_2 d\mathbf{r}_1 d\mathbf{r}_2 d\varphi_1 d\varphi_2, \end{aligned} \quad (4)$$

where $\boldsymbol{\rho}_i$ ($i=1, 2$) and θ_i ($i=1, 2$) denote the radial and azimuthal (angle) coordinates in the receiver plane, respectively. A , B , and D denote the transfer matrix elements of the ABCD optical system, and $k = 2\pi/\lambda$ stands for the wavenumber with wavelength λ . The range of integration with respect to the variable φ is from $\alpha/2$ to $2\pi-\alpha/2$ and is caused by the existence of the sector-shaped opaque obstacle. Then, we normalize the cross-spectral density function and obtain the degree of coherence function⁴³:

$$\mu(\boldsymbol{\rho}_1, \boldsymbol{\rho}_2) = W(\boldsymbol{\rho}_1, \boldsymbol{\rho}_2) / \sqrt{W(\boldsymbol{\rho}_1, \boldsymbol{\rho}_1) W(\boldsymbol{\rho}_2, \boldsymbol{\rho}_2)}. \quad (5)$$

In particular, when $\alpha=0$, Eqs. (4) and (5) reduce to the situation without obstacle occlusion. It is well known that turbulent atmosphere can provide a kind of phase disturbance to the transmitted light. To study the propagation of light waves in turbulent atmosphere, we choose the most widely used multiphase screen

method^{30,36}, i.e., first decompose an incoming beam into a series of random electric fields, and then let these random electric fields pass through the turbulent atmosphere. During propagation, the turbulence is equivalent to a collection of thin random phase screens with the desired turbulence statistics. We will briefly introduce the method below and refer to ref.^{30,36} for details.

Consider a physically realizable PCLG beam with a cross-phase, whose cross-spectral density function given by Eq. (1) can also be represented by the following integral:

$$W(\mathbf{r}_1, \mathbf{r}_2) = \tau(\mathbf{r}_1) \tau^*(\mathbf{r}_2) \int P(\mathbf{v}_1, \mathbf{v}_2) \times \exp[-i2\pi(\mathbf{v}_2 \cdot \mathbf{r}_2 - \mathbf{v}_1 \cdot \mathbf{r}_1)] d^2 \mathbf{v}_1 d^2 \mathbf{v}_2, \quad (6)$$

with

$$\tau(\mathbf{r}) = \tau_0(\mathbf{r}) \exp(iu\mathbf{r}), \quad (7)$$

and

$$P(\mathbf{v}_1, \mathbf{v}_2) = \sqrt{P(\mathbf{v}_1)} \sqrt{P(\mathbf{v}_2)} \delta(\mathbf{v}_1 - \mathbf{v}_2), \quad (8)$$

where $\tau(\mathbf{r})$ is the new complex function and $P(\mathbf{v}) = (2\pi\sigma^2) \exp(-2\pi^2\sigma^2 \mathbf{v}^2)$ is a non-negative function that refers to the power spectral density. The Dirac function δ is rewritten as:

$$\delta(\mathbf{v}_1 - \mathbf{v}_2) = \langle C_n(\mathbf{v}_1) C_n^*(\mathbf{v}_2) \rangle, \quad (9)$$

where the angular bracket stands for the ensemble average and $C_n(\mathbf{v})$ denotes the random complex function that can be viewed as the field of the white noise⁴⁴. Here, we assume the beam is statistically stationary, i.e., the ensemble averaging over the random fields can be replaced by the incoherent superposition of instantaneous random realizations, and substitute Eqs. (7-9) into Eq. (6), and obtain:

$$W(\mathbf{r}_1, \mathbf{r}_2) = \langle E_n(\mathbf{r}_1) E_n^*(\mathbf{r}_2) \rangle \approx \frac{1}{N} \sum_{n=1}^N E_n(\mathbf{r}_1) E_n^*(\mathbf{r}_2), \quad (10)$$

with

$$E_n(\mathbf{r}) = \tau(\mathbf{r}) T_n(\mathbf{r}), \quad (11)$$

and

$$T_n(\mathbf{r}) = \text{FFT} \left[\sqrt{P(\mathbf{v})} C_n(\mathbf{v}) \right], \quad (12)$$

where $\text{FFT}[\cdot]$ denotes the symbol of Fourier transform, $T_n(\mathbf{r})$ stands for the instantaneous electric field that represents one realization of an incoming beam. That is, the generation of a PCLG beam with a cross-phase can be treated as the fully coherent portion $\tau(\mathbf{r})$, illuminating

the random complex screens $T_n(\mathbf{r})$. To numerically simulate the propagation of light beams through turbulent atmosphere, we need to equate the continuous turbulent medium to some random phase screens with equal intervals, placed in the direction of light wave transmission. The interval between two adjacent phase screens is $\Delta z = z_1/M$, where z_1 is the distance from the light source plane to the last random phase screen, and M is the number of random phase screens. Here we choose $z_1=1$ m and $M=5$ to satisfy the restriction condition of the Rytov variance.

The scenario for simulating the propagation of a PCLG beam with a cross-phase in the presence of turbulent atmosphere is as follows. The incident electric field of the beam source $E_1(\mathbf{r}_1)$ propagates a distance Δz in free space, and becomes $E_1'(\mathbf{r}_2)$ at the first phase screen. Then, the propagated electric field will be modulated by the random phase screen that represents the accumulated turbulence effect over the distance Δz , i.e., $E_2(\mathbf{r}_2) = E_1'(\mathbf{r}_2) \exp[i\theta_1(\mathbf{r}_2)]$, where θ_1 denotes the accumulated phase fluctuations induced by the turbulence over the distance Δz .

The following propagation steps just repeat the first propagation step, until the beam reaches the last phase screen. The incident electric field is expressed as $E_{m+1}(\mathbf{r}_{m+1}) = E_m'(\mathbf{r}_{m+1}) \exp[i\theta_m(\mathbf{r}_{m+1})]$. Finally, the light field is focused by a collecting lens and arrives at the detector in the detection plane.

The method for synthesizing θ_m is similar to that for the synthesis of the complex screen described above, but uses the power spectrum $\Phi_n(\boldsymbol{\kappa})$ of the turbulence-induced refractive index fluctuations. The relationship between $\Phi_n(\boldsymbol{\kappa})$ and the spectrum $\Phi_\theta(\boldsymbol{\kappa})$ of the phase screen induced by turbulence is given by the following formula³⁶:

$$\Phi_\theta(\boldsymbol{\kappa}) = 2\pi\Delta z k^2 \Phi_n(\boldsymbol{\kappa}), \quad (13)$$

where $\boldsymbol{\kappa} = 2\pi(f_x, f_y)$ denotes the spatial frequency vector that forms a Fourier transform with the spatial coordinate \mathbf{r} . Following the same procedure for synthesis of the complex screen for partially coherent beams, Eq. (13) is first multiplied by a random complex function $C_m(\boldsymbol{\kappa})$; then we take a Fourier transform of the result. The real or imaginary parts of the result each represent a valid realization of the turbulence screen phase, i.e., $\theta_m(\mathbf{r}_{m+1}) = \text{Re}\{\text{FFT}[C_m(\boldsymbol{\kappa})\Phi_\theta(\boldsymbol{\kappa})]\}$, where Re denotes the real part operation.

In our simulation, we limit the refractive index spectral density to the well-known Kolmogorov spectrum,

defined as³⁶:

$$\Phi_n(\boldsymbol{\kappa}) = 0.033C_n^2\boldsymbol{\kappa}^{-11/3}, \quad (14)$$

where C_n^2 is the atmospheric refractive index structure constant which is a weight factor for the strength of the turbulence.

The effect of a cross-phase on the degree of coherence of a PCLG beam

In this section, we will introduce a concise and efficient principle to probe the OAM of a partially coherent vortex beam. In this protocol, we employ only a cross-phase. The beam, modulated by the cross-phase, propagates to the Fraunhofer zone. Due to the mode-conversion property induced by the cross-phase, the OAM (topological charge) information is contained in the degree of coherence structure of a partially coherent vortex beam in the form of a set of distinct and separated ring singularities. Thus, by measuring the distribution of degree of coherence, we can extract the topological charge information. It is worth noting that this method is applicable not only for detection in free space, but also for detection in the transmission environment with obstacles and a turbulent atmosphere. This is due to the self-reconstruction property of the spatial-coherence structure embedded with the cross-phase. A schematic of the proposed protocol is illustrated in Fig. 1.

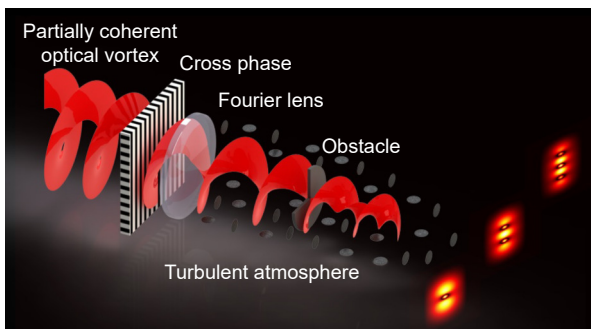


Fig. 1 | Schematic diagram probing the OAM of a partially coherent optical vortex via a cross-phase.

To demonstrate the effect of the above protocol, we will study the degree of coherence function of a PCLG beam embedded with and without cross-phase, which passes through a thin lens with focal length f and then arrives at an output plane. The distance from the thin lens to the output plane is z . The transfer matrix between the source plane and the output plane reads as:

$$\begin{pmatrix} A & B \\ C & D \end{pmatrix} = \begin{pmatrix} 1 & z \\ 0 & 1 \end{pmatrix} \begin{pmatrix} 1 & 0 \\ -1/f & 1 \end{pmatrix} = \begin{pmatrix} 1 - z/f & z \\ -1/f & 1 \end{pmatrix}. \quad (15)$$

We show in Fig. 2 the numerical calculation results of the modulus of the degree of coherence $|\mu(\boldsymbol{\rho}, -\boldsymbol{\rho})|$ of a PCLG beam with different values of u for different topological charges in the focal plane. The parameters are chosen as $\omega=\sigma=1$ mm, $p=0$, $\lambda=632.8$ nm and $z=f=400$ mm unless otherwise specified. The first column is set for comparison and corresponds to the cases without cross-phase (i.e., $u=0$ mm⁻²). One finds that there are unique concentric dark ring structures in the spatial distribution of $|\mu(\boldsymbol{\rho}, -\boldsymbol{\rho})|$ and its number is exactly corresponding to the magnitude of the topological charge carried by the beam [see Fig. 2(a1), 2(b1), 2(c1) and 2(d1)], which is consistent with the earlier studies²⁷⁻²⁸. Thus, this coherence structure (i.e., a spatial distribution of $|\mu(\boldsymbol{\rho}, -\boldsymbol{\rho})|$), carrying topological charge information, can be used for information encryption⁴⁵. It is worth noting that with the increase of u , the cross-phase can cause splitting in the spatial distribution of $|\mu(\boldsymbol{\rho}, -\boldsymbol{\rho})|$, and the concentric dark ring distribution will gradually evolve into the distribution with multiple isolated dark rings. The number of isolated dark rings ($N_1=1, 2, 3$ and 4) is equal to the magnitude of the carried topological charge ($|l|=1, 2, 3$ and 4) [see Fig. 2(a3), 2(b3), 2(c3) and 2(d3)]. The sign of topological charge is determined by the arrangement direction of separated dark rings⁴⁶. The vertical direction indicates that the topological charge is positive and the horizontal direction indicates that the topological charge is negative.

Above splitting property can be explained by the pseudo-mode superposition principle⁴⁷ and cross-phase induced mode conversion³⁷. Figure 3 shows the schematic diagram of the pseudo-mode superposition principle and cross-phase induced coherence structure splitting. The cross-spectral density function given by Eq. (6) can be constructed from a certain number of individual Laguerre Gaussian mode superpositions with different mode weight [see Fig. 3(a), here we take $K=400$ sub-modes], and more details could be found in the supplementary material. Either free space or a turbulent atmosphere is a linear space, therefore, the propagation properties of a PCLG beam can be viewed as the result of the superposition of sub-pseudo-modes propagated separately (the analytical expression for the propagation of individual pseudo-mode is shown in the Supplement).

Following ref.³⁷, the fully coherent Laguerre Gaussian mode gradually evolve into Hermitian Gaussian mode with the help of the cross-phase. Therefore, we can see from Fig. 3(a) and Fig. 3(b) that each individual Laguerre Gaussian mode with doughnut-shaped distribution in the source plane splits on propagation due to the cross-phase, and finally present the Hermitian Gaussian-like patterns at the focal plane. Further, the number of main lobe spots obeys $N_2 = |l|+1$ (here $l=1$). It is worth noting that the light intensity distribution of each sub-mode is basically the same except the position and mode weight, and the total light intensity of the superimposed composite light field is also consistent with the light intensity distribution of the sub-modes [see Fig. 3(b) and Fig. 3(c)]. Similarly, the spatial distribution of $|\mu(\rho, -\rho)|$ of the superimposed synthetic light field (i.e., a PCLG beam) also maintains the Hermitian Gaussian-like profile. For example, in Fig. 3(d), there are obvious two (i.e., $l+1$) main lobes (see the part marked by the green line), and an isolated dark ring structure is formed between each of the two main lobes. The splitting of individual Laguerre Gaussian mode is the formation mechanism of dark ring structure. Therefore, due to the cross-phase, we can see that the spatial distribution of $|\mu(\rho, -\rho)|$ of a PCLG beam with larger topological charge will gradually evolve into the distribution with multiple isolated dark rings [see Fig. 2(b3), 2(c3) and 2(d3)].

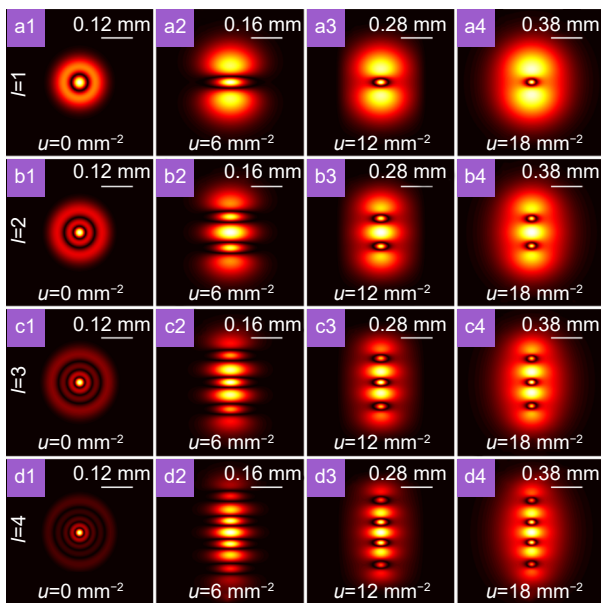


Fig. 2 | The evolution for the modulus of the degree of coherence of a partially coherent Laguerre Gaussian beam carrying different topological charges in the focal plane versus the values of u .

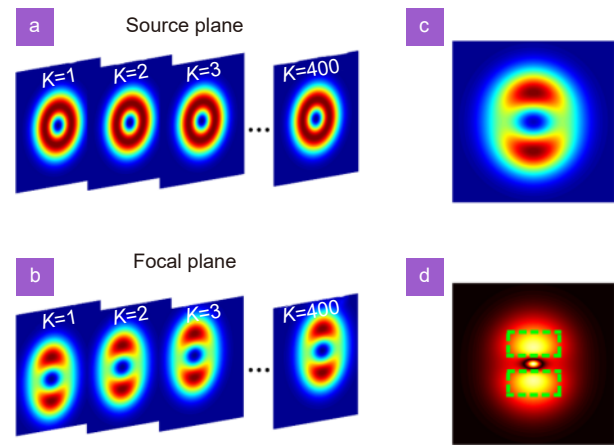


Fig. 3 | The schematic diagram of the pseudo-mode superposition principle and cross-phase induced spatial-coherence structure splitting. (a) The intensity distribution of each individual Laguerre Gaussian sub-mode embedded with cross-phase for $u=12 \text{ mm}^{-2}$ and $l=1$ in the source plane. (b) The intensity distribution of each individual Laguerre Gaussian sub-mode embedded with cross-phase for $u=12 \text{ mm}^{-2}$ and $l=1$ in the focal plane. (c) The average intensity of a partially coherent Laguerre Gaussian beam embedded with cross-phase for $u=12 \text{ mm}^{-2}$ and $l=1$ in the focal plane. (d) The distribution of modulus of the degree of coherence of a partially coherent Laguerre Gaussian beam embedded with cross-phase for $u=12 \text{ mm}^{-2}$ and $l=1$ in the focal plane. The green line is used to mark the main lobe structure.

By comparing the first and third columns, it is obvious that the distribution embedded with cross-phase is more intuitive and recognizable for measuring topological charge than that without cross-phase, especially for the case of beams carrying higher topological charge (e.g., $l=4$). As u further increases, the isolated dark rings gradually get smaller [see Fig. 2(a4), 2(b4), 2(c4) and 2(d4)]. This is due to the beam splitting and self-dispersion properties induced by the cross-phase. It is worth noting that this splitting property holds for different coherence conditions. The lower the coherence, the larger the value of u required. Therefore, this also reveals to us a new phase coupling effect, namely: cross-phase enables the separation of the coherent singularities induced by the vortex phase, and this cross-phase based splitting effect opens the door for efficient measurement of the topological charge in partially coherent vortex beams.

Robust measurement of the topological charge of a PCLG beam under amplitude perturbation and phase perturbation

In this section, we will investigate the spatial-coherence structure of a PCLG beam under amplitude/phase perturbation and display the anti-amplitude/anti-phase

disturbance characteristics of the spatial-coherence structure with the help of the cross-phase.

We first place the obstacles with occlusion angle $\alpha = \pi/3$ and $\alpha = \pi/2$ in the source plane of a PCLG beam and investigate the corresponding spatial distribution of $|\mu(\rho, -\rho)|$ of a PCLG beam in the output plane. We calculate in Fig. 4(a1–a4) and 4(b1–b4) the spatial distribution of $|\mu(\rho, -\rho)|$ of a PCLG beam without cross-phase in the focal plane when the obstacle is placed in the source plane. One finds that in the absence of cross-phase (i.e., $u=0 \text{ mm}^{-2}$), the spatial distribution of $|\mu(\rho, -\rho)|$ of a PCLG beam in the focal plane is severely damaged when it is partially blocked by an obstacle at the light source, implying a large loss of information carried by the spatial distribution of $|\mu(\rho, -\rho)|$. Specifically, compared to the case when the obstacle is removed in the first column of Fig. 2 (i.e., $\alpha=0$), the occlusion due to obstacles destroys the original concentric dark ring structure, resulting in the discontinuity of the dark rings. Especially for the case with higher topological charge, the spatial distribution of $|\mu(\rho, -\rho)|$ will eventually show speckle distribution characteristics [Fig. 4(a4, b4)], which makes it difficult or even impossible to extract topological charge information from the spatial distribution of $|\mu(\rho, -\rho)|$.

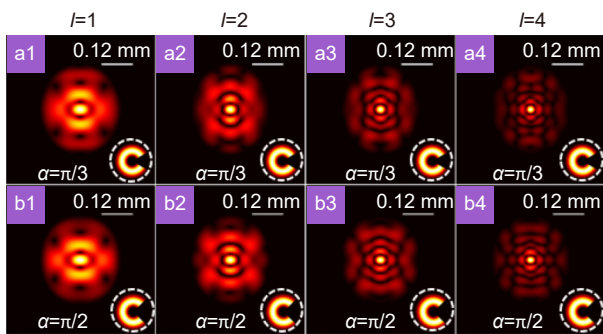


Fig. 4 | The distributions of modulus of the degree of coherence of partially coherent Laguerre Gaussian beams without cross-phase in the focal plane when obstacles with different occlusion angles α are placed in the source plane. The illustrations in the lower right corner represents the corresponding intensity distribution in the source plane when obstacles with different occlusion angles α are placed in the source plane.

To be able to identify the topological charge under the disturbance of the amplitude type obstacle above, we coupled the cross-phase into a PCLG beam. Figure 5 shows the effect of the cross-phase on the spatial distribution of $|\mu(\rho, -\rho)|$ under the amplitude perturbation. By comparing Fig. 2 [Figs 2(a3), 2(b3), 2(c3) and 2(d3)] and Fig. 5, it can be readily seen that with the introduction of

a cross-phase, the spatial distribution of $|\mu(\rho, -\rho)|$ in the presence of the obstacle basically maintains the original characteristic distribution without the obstacle, i.e., possessing a set of distinct and separated dark rings equal in number to the magnitude of the topological charge. By comparing the results in Fig. 5 with the distributions arising from severe damage by obstacles, as shown in Fig. 4, shows that the cross-phase endows a PCLG beam with a certain ability to resist amplitude perturbation. On the one hand, this is because in such cases, the obstacle transmittance area is larger than the spatial-coherence area of the partially coherent vortex source (approximately 1 mm^2), obeying the condition for beam self-reconstruction^{16,31}. On the other hand, this is because the splitting of the light intensity caused by cross-phase makes the spot larger thereby weakening the diffraction effect caused by obstacles, making it robust against the obstruction of obstacles. Thus, by modulating the cross-phase, the topological charge of the partially coherent vortex source can still be detected in case of amplitude disturbance.

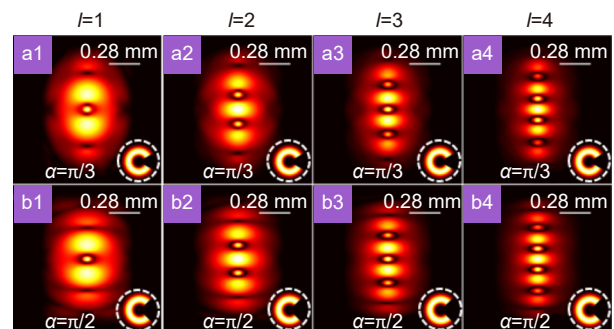


Fig. 5 | The distributions of modulus of the degree of coherence of partially coherent Laguerre Gaussian beams with cross-phase ($u=12 \text{ mm}^{-2}$) in the focal plane when obstacles with different occlusion angles α are placed in the source plane. The illustrations in the lower right corner represents the corresponding intensity distributions in the source plane when obstacles with different occlusion angles α are placed in the source plane.

To further reveal the effect of the cross-phase on the spatial-coherence structure, we show in Fig. 6 the spatial distribution of $|\mu(\rho, -\rho)|$ of PCLG beams with and without cross-phase for different topological charges and occlusion angles of the obstacle (i.e., $\alpha = 0$, $\alpha = \pi/2$) in the presence of turbulence. The first row and the second row of Fig. 6 show the spatial distribution of $|\mu(\rho, -\rho)|$ of PCLG beams carrying different topological charges without cross-phase under phase perturbation and the common disturbance of phase and amplitude,

respectively. The structure constant for the turbulence is chosen as $C_n^2 = 3 \times 10^{-11} \text{ m}^{-2/3}$. Compared to the case without phase perturbation in the first column of Fig. 2, one finds that due to the influence of phase disturbance (turbulence), the original circular symmetry structure is obviously distorted in Fig. 6(a1–a4). Furthermore, we found that under the joint intervention of amplitude disturbance (obstacle) and phase disturbance (turbulence), the spatial distribution of $|\mu(\rho, -\rho)|$ is much more severely damaged [see Fig. 6(b1–b4)] than when they exist alone, making it impossible for us to obtain topological charge information. This is due to the complex effect of obstacles and the turbulent atmosphere on the vortex phase, which leads to the annihilation and generation of coherent vortices, destroying the concentric ring distribution structure that can originally represent topological charge information.

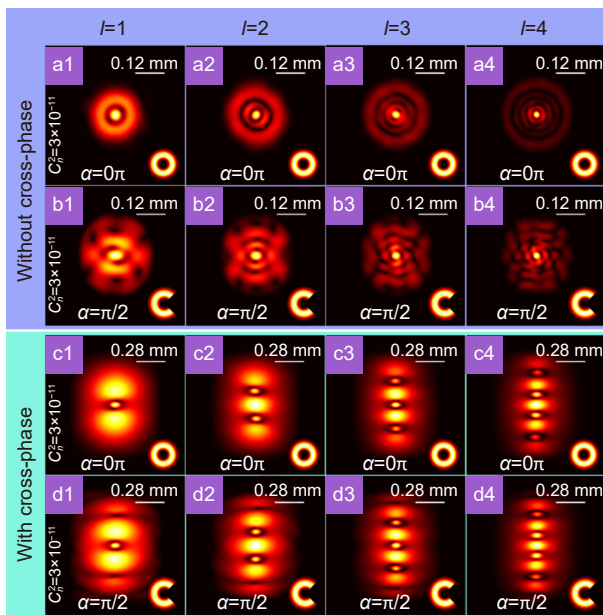


Fig. 6 | (a1–a4) The distributions of modulus of the degree of coherence of partially coherent Laguerre Gaussian beams without cross-phase in the focal plane in the presence of turbulence. **(b1–b4)** The distributions of modulus of the degree of coherence partially coherent Laguerre Gaussian beams without cross-phase in the focal plane in the presence of an obstacle with occlusion angle $\alpha = \pi/2$ and turbulence. **(c1–c4)** The distributions of modulus of the degree of coherence of partially coherent Laguerre Gaussian beams with cross-phase in the focal plane in the presence of turbulence. **(d1–d4)** The distributions of modulus of the degree of coherence of partially coherent Laguerre Gaussian beams with cross-phase in the focal plane in the presence of an obstacle with occlusion angle $\alpha = \pi/2$ and turbulence. The illustrations in the lower right corner represents the corresponding intensity distributions in the source plane obstructed by obstacles with different occlusion angles α .

Fortunately, after we additionally introduce a cross-phase, it can be seen from Fig. 6(c1–d4) that the spatial distribution of $|\mu(\rho, -\rho)|$ still maintains the original distribution characteristics (i.e., the cases without perturbations) even under the double perturbations of amplitude and phase. Especially the structural distribution, used to characterize topological charges, is still clearly visible (i.e., $N_1 = |l|$). This is because in such cases, the improvement in the self-healing ability and the anti-diffraction property of the beam source brought about by the cross-phase are enough to resist the adverse influence of the annihilation and generation of coherent vortices. In other words, cross-phase resists the distortion and destruction caused by occlusion and turbulence, the coherent structure can still be stably transmitted to the far field, thereby achieving effective measurement of topological charges, even if the amplitude and phase are disturbed.

Robust measurement of the topological charge of a PCLG beam under amplitude and phase perturbations: experimental verification

In this section, we carry out a proof-of-principle experiment to show the robust measurement of the topological charge in the far-field transmission. Figure 7(a) shows the experimental setup for generating a PCLG beam carrying a cross-phase with different values of u and measuring its distribution of modulus of the degree of coherence in a complex environmental path. A coherent beam emitted by a He-Ne laser at a wavelength of $\lambda = 632.8 \text{ nm}$ passes through a neutral density filter and a linear polarizer and is then focused by a lens L_1 ($f_1 = 250 \text{ mm}$) onto a rotating ground glass disk. Based on the van Cittert–Zernike theorem, the generated incoherent beam becomes a Gaussian Schell-model beam after passing through a collimation lens L_2 ($f_2 = 250 \text{ mm}$) and a Gaussian amplitude filter⁴⁸. Then this beam arrives at a beam splitter. The transmitted beam goes towards the spatial light modulator, which acts as a phase grating, to load the required amplitude and phase information designed by the method of computer-generated holograms⁴⁶. The modulated beam passes through a 4-f optical system consisting of lenses L_3 and L_4 ($f_3 = f_4 = 250 \text{ mm}$) to select the +1st order with the help of the circular aperture. The rear focal plane of L_4 is regarded as the source plane of the generated PCLG beam carrying the cross-phase. The generated beam passes through a sector shaped obstacle and a thin lens L_5 ($f_5 = 400 \text{ mm}$) and then arrives at a

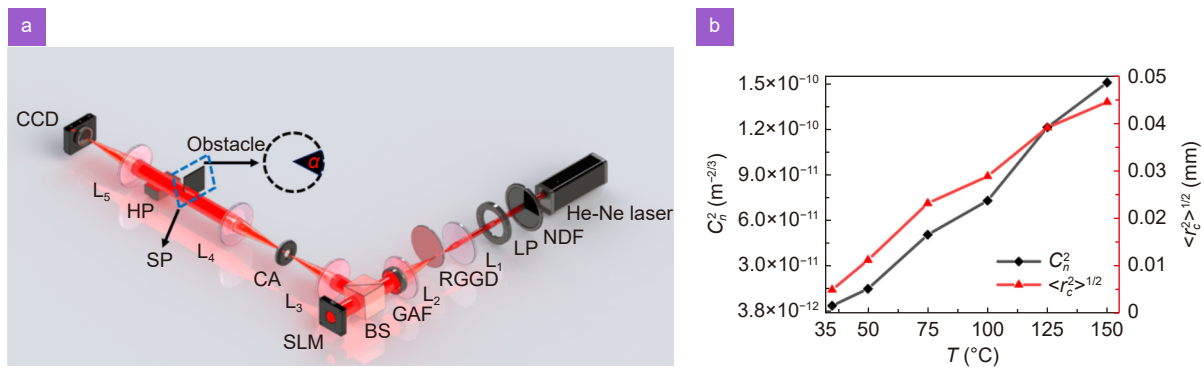


Fig. 7 | (a) Experiment setup for the generation of a partially coherent Laguerre Gaussian beam with a controllable cross-phase and the measurement of the distribution of modulus of the degree of coherence of this beam, when obstructed by an obstacle in the far field propagation in free space (without hot plate) as well as in a turbulent atmosphere (with hot plate). Laser, a He-Ne laser with wavelength 632.8 nm; NDF, neutral density filter; LP, linear polarizer; RGGD, rotating ground glass disk; L_1 , L_2 , L_3 , L_4 , L_5 , thin lenses; GAF, Gaussian amplitude filter; BS, beam splitter; SLM, spatial light modulator; CA, circular aperture; SP, source plane; HP, hot plate; CCD, charge-coupled device. (b) Measured atmospheric refractive index structure constant C_n^2 and beam wander $\langle r_c^2 \rangle^{1/2}$ through the turbulence cell as a function of the control temperature of the hot plate.

charge coupled device located in the focal plane of L_5 , which is used to measure the distribution of modulus of the degree of coherence³². Here the sector shaped obstacle is used to realize the amplitude perturbation. In addition, to study the influence of turbulence, a hot plate with a length of 300 mm along the transmission path will be placed between the source plane and L_5 ³⁰. The hot plate controls the strength of the turbulence by adjusting its temperature setting. According to the protocol described by Vallone et al.⁴⁹, we have measured the refractive index structure constant and beam wander corresponding to different hot plate temperatures under the current experimental configuration. The quantitative relationship between the strength of turbulence and hot plate temperature has been given in Fig. 7(b). The results show that the higher the temperature, the stronger the turbulence generated, that is, the corresponding atmospheric refractive index structure constant C_n^2 and beam wander $\langle r_c^2 \rangle^{1/2}$ are larger.

In the experiment, obstacles with different central occlusion angles α are placed in the source plane of a PCLG beam carrying a cross-phase for $u=12 \text{ mm}^{-2}$. The experimental results for the modulus of the degree of coherence $|\mu(\rho, -\rho)|$ in the focal plane for different values of α and topological charges are presented in Fig. 8. The beam parameters set in the experiment are $\omega=\sigma=1 \text{ mm}$, $p=0$, $l=1, 2, 3, 4$. One finds from Fig. 8 that our experimental results agree well with our theoretical predictions in Fig. 2 and Fig. 5, i.e., when the spatial-coherence area is smaller than the obstacle transmittance area, due to the effect of the cross-phase, the distribution of $|\mu(\rho, -\rho)|$ always possesses a set of distinct and separated dark

rings equal in number to the magnitude of the topological charge, regardless of occlusion. The results indicate that the cross-phase makes that the spatial-coherence structure of a partially coherent vortex beam can indeed be used for transmitting the topological charge information in the transmission link with obstacles.

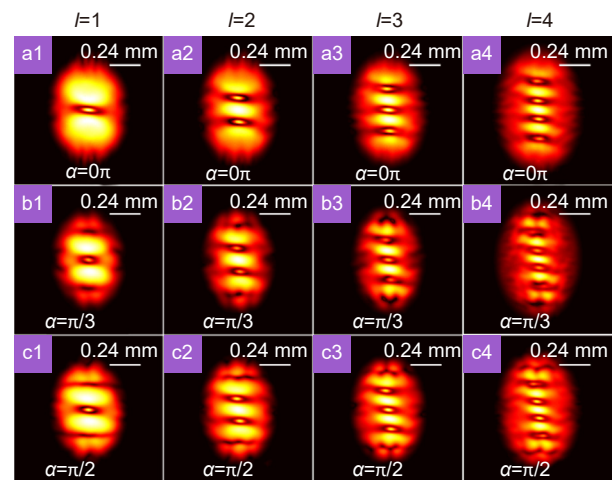


Fig. 8 | The experimental results for the modulus of the degree of coherence of a partially coherent Laguerre Gaussian beam carrying a cross-phase for $u=12 \text{ mm}^{-2}$ in the focal plane. (a1–a4) The experimental results for the cases with different topological charges l when the obstacle is removed. (b1–b4) The experimental results for the cases with different topological charges l when the obstacle with occlusion angle $\alpha=\pi/3$ is placed in the source plane. (c1–c4) The experimental results for the cases with different topological charges l when the obstacle with occlusion angle $\alpha=\pi/2$ is placed in the source plane.

To further verify the robustness of its transmission, we also conducted corresponding experiments under turbulence perturbation. Figure 9 presents the experimental

results for the distribution of modulus of the degree of coherence of a PCLG beam, carrying a cross-phase with $u=12 \text{ mm}^{-2}$, obstructed by an obstacle with occlusion angle α in the presence of turbulence with temperature $T=50 \text{ }^\circ\text{C}$ in the focal plane for different values of α and l . The experimental results are consistent with our prediction that the spatial-coherence structure can stably transmit and retain topological charge information, regardless of the presence of atmospheric turbulence and obstacles in the transmission link. This also proves that in such cases, the self-healing ability and anti-diffraction properties conferred by the cross-phase are indeed enough to help spatial-coherence structure resist the negative effects induced by obstacles and turbulent atmosphere. Afterwards, we examine the effect of turbulence condition on the measurements by adjusting the hot plate temperature, and the experimental results are shown in Fig. 10. It is found that in all cases, the topological charge can be recognized well and the measurement accuracy is robust within $100 \text{ }^\circ\text{C}$. This indicates that the cross-phase makes the modulus of the degree of coherence a robust parameter for transmitting the topological charge/OAM information. In addition, the consistency of the measurement results under the above four

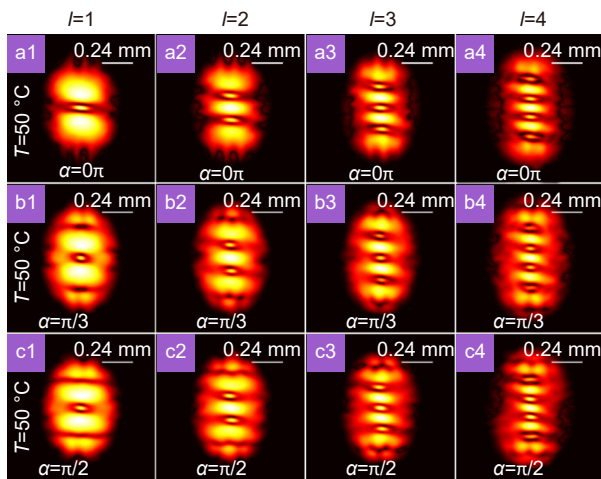


Fig. 9 | Experimental results for the effect of the obstacle and turbulence on the modulus of the degree of coherence of a partially coherent Laguerre Gaussian beam carrying a cross-phase in the focal plane for $u=12 \text{ mm}^{-2}$. (a1–a4) The experimental results for the cases in the presence of turbulence with temperature $T=50 \text{ }^\circ\text{C}$ when the obstacle is removed. (b1–b4) The experimental results for the cases in the presence of turbulence with temperature $T=50 \text{ }^\circ\text{C}$ when the obstacle with occlusion angle $\alpha=\pi/3$ is placed in the source plane. (c1–c4) The experimental results for the cases in the presence of turbulence with temperature $T=50 \text{ }^\circ\text{C}$ when the obstacle with occlusion angle $\alpha=\pi/2$ is placed in the source plane.

different transmission conditions (in free space, in the transmission link with an obstacle, in the transmission link with a turbulent atmosphere and in the transmission link with both obstacle and a turbulent atmosphere) illustrates the robustness of our scheme.

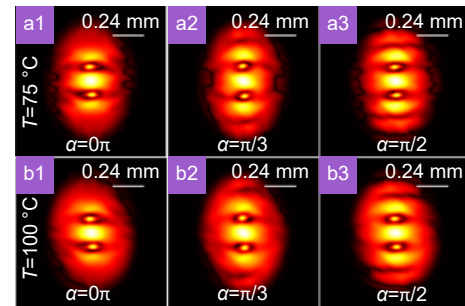


Fig. 10 | Experimental results for the effect of the temperature on the modulus of the degree of coherence of a partially coherent Laguerre Gaussian beam carrying a cross-phase for $l=2$ and $u=12 \text{ mm}^{-2}$ in the focal plane. (a1–a3) The experimental results for the cases in the presence of turbulence with temperature $T=75 \text{ }^\circ\text{C}$ when obstacles with different occlusion angles α are placed in the source plane. (b1–b3) The experimental results for the cases in the presence of turbulence with temperature $T=100 \text{ }^\circ\text{C}$ when obstacles with different occlusion angles α are placed in the source plane.

Conclusions

In summary, we have presented, with the help of the cross-phase, a robust protocol that significantly reduces the requirements for the pertinent transmission environment for a measurement of the topological charge of a partially coherent Laguerre Gaussian beam. Measurements of the number of dark rings in the modulus of the degree of coherence are conducted to characterize the topological charge of the generated partially coherent Laguerre Gaussian beam. The results revealed that the magnitude of the topological charge is equal to the number of isolated dark rings. Furthermore, we found that the introduction of a cross-phase enables the topological charge of a partially coherent Laguerre Gaussian beam to be detected in different perturbing environments (e.g., obstacles occlusion, atmospheric turbulence disturbance, or even both), which greatly improves the robustness of the measurement. The experimental results agree well with the theoretical predictions. Our results provide a convenient way to detect the topological charge of a partially coherent vortex beam under amplitude and phase perturbations and hopefully will pave the way to optical communication in complicated natural environments.

References

- Gbur GJ. *Singular Optics* (CRC Press, Boca Raton, 2017).
- Willner AE, Huang H, Yan Y et al. Optical communications using orbital angular momentum beams. *Adv Opt Photonics* 7, 66 (2015).
- He H, Friese MEJ, Heckenberg NR et al. Direct observation of transfer of angular momentum to absorptive particles from a laser beam with a phase singularity. *Phys Rev Lett* 75, 826–829 (1995).
- Paterson L, MacDonald MP, Arlt J et al. Controlled rotation of optically trapped microscopic particles. *Science* 292, 912–914 (2001).
- Yang YJ, Ren YX, Chen MZ et al. Optical trapping with structured light: a review. *Adv Photonics* 3, 034001 (2021).
- Tamburini F, Anzolin G, Umbriaco G et al. Overcoming the rayleigh criterion limit with optical vortices. *Phys Rev Lett* 97, 163903 (2006).
- Qiu XD, Li FS, Zhang WH et al. Spiral phase contrast imaging in nonlinear optics: seeing phase objects using invisible illumination. *Optica* 5, 208–212 (2018).
- Lavery MPJ, Speirits FC, Barnett SM et al. Detection of a spinning object using light's orbital angular momentum. *Science* 341, 537–540 (2013).
- Kong LJ, Zhang WX, Li P et al. High capacity topological coding based on nested vortex knots and links. *Nat Commun* 13, 2705 (2022).
- Wen YH, Chremmos I, Chen YJ et al. Arbitrary multiplication and division of the orbital angular momentum of light. *Phys Rev Lett* 124, 213901 (2020).
- Fang XY, Ren HR, Gu M. Orbital angular momentum holography for high-security encryption. *Nat Photonics* 14, 102–108 (2020).
- Andrews LC, Phillips RL. *Laser Beam Propagation through Random Media* 2nd ed (SPIE Press, Bellingham, 2005).
- Popoff S, Leroose G, Fink M et al. Image transmission through an opaque material. *Nat Commun* 1, 81 (2010).
- Zeng J, Liu XL, Zhao CL et al. Spiral spectrum of a Laguerre-Gaussian beam propagating in anisotropic non-Kolmogorov turbulent atmosphere along horizontal path. *Opt Express* 27, 25342–25356 (2019).
- Ricklin JC, Davidson FM. Atmospheric turbulence effects on a partially coherent Gaussian beam: implications for free-space laser communication. *J Opt Soc Am A* 19, 1794–1802 (2002).
- Wang F, Chen YH, Liu XL et al. Self-reconstruction of partially coherent light beams scattered by opaque obstacles. *Opt Express* 24, 23735–23746 (2016).
- Korotkova O, Gbur G. Applications of optical coherence theory. *Prog Opt* 65, 43–104 (2020).
- Chen YH, Ponomarenko SA, Cai YJ. Experimental generation of optical coherence lattices. *Appl Phys Lett* 109, 061107 (2016).
- Liu XL, Shen Y, Liu L et al. Experimental demonstration of vortex phase-induced reduction in scintillation of a partially coherent beam. *Opt Lett* 38, 5323–5326 (2013).
- Wang HT, Wang H, Ruan QF et al. Coloured vortex beams with incoherent white light illumination. *Nat Nanotechnol* 18, 264–272 (2023).
- Yang GL, Su JH, Li Y et al. A study of resolution improvement in Noncoherent optical coherence imaging. *Adv Math Phys* 2022, 3232323 (2022).
- Zhao CL, Cai YJ. Trapping two types of particles using a focused partially coherent elegant Laguerre-Gaussian beam. *Opt Lett* 36, 2251–2253 (2011).
- Chen YH, Wang F, Cai YJ. Partially coherent light beam shaping via complex spatial coherence structure engineering. *Adv Phys X* 7, 2009742 (2022).
- Bai YH, Lv HR, Fu X et al. Vortex beam: generation and detection of orbital angular momentum [Invited]. *Chin Opt Lett* 20, 012601 (2022).
- Liu XL, Zeng J, Cai YJ. Review on vortex beams with low spatial coherence. *Adv Phys X* 4, 1626766 (2019).
- Zhao CL, Wang F, Dong Y et al. Effect of spatial coherence on determining the topological charge of a vortex beam. *Appl Phys Lett* 101, 261104 (2012).
- Yang YJ, Mazilu M, Dholakia K. Measuring the orbital angular momentum of partially coherent optical vortices through singularities in their cross-spectral density functions. *Opt Lett* 37, 4949–4951 (2012).
- Liu RF, Wang FR, Chen DX et al. Measuring mode indices of a partially coherent vortex beam with Hanbury brown and Twiss type experiment. *Appl Phys Lett* 108, 051107 (2016).
- Liu XL, Wu TF, Liu L et al. Experimental determination of the azimuthal and radial mode orders of a partially coherent LGpl beam. *Chin Opt Lett* 3, 030002 (2017).
- Liu YL, Chen YH, Wang F et al. Robust far-field imaging by spatial coherence engineering. *Opto-Electron Adv* 4, 210027 (2021).
- Liu YL, Zhang X, Dong Z et al. Robust far-field optical image transmission with structured random light beams. *Phys Rev Appl* 17, 024043 (2022).
- Liu XL, Peng XF, Liu L et al. Self-reconstruction of the degree of coherence of a partially coherent vortex beam obstructed by an opaque obstacle. *Appl Phys Lett* 110, 181104 (2017).
- Peng XF, Liu L, Wang F et al. Twisted Laguerre-Gaussian Schell-model beam and its orbital angular moment. *Opt Express* 26, 33956–33969 (2018).
- Gbur G, Tyson RK. Vortex beam propagation through atmospheric turbulence and topological charge conservation. *J Opt Soc Am A* 25, 225–230 (2008).
- Li JH, Zeng J, Duan ML. Classification of coherent vortices creation and distance of topological charge conservation in non-Kolmogorov atmospheric turbulence. *Opt Express* 23, 11556–11565 (2015).
- Yu JY, Huang Y, Wang F et al. Scintillation properties of a partially coherent vector beam with vortex phase in turbulent atmosphere. *Opt Express* 27, 26676–26688 (2019).
- Liang G, Wang Q. Controllable conversion between Hermite Gaussian and Laguerre Gaussian modes due to cross phase. *Opt Express* 27, 10684–10691 (2019).
- Wan LP, Zhao DM. Controllable rotating Gaussian Schell-model beams. *Opt Lett* 44, 735–738 (2019).
- Ren Y, Wang C, Liu T et al. Polygonal shaping and multi-singularity manipulation of optical vortices via high-order cross-phase. *Opt Express* 28, 26257–26266 (2020).
- Xin L, Li ZQ, Monfared YE et al. Flexible autofocusing properties of ring Pearcey beams by means of a cross phase. *Opt Lett* 46, 70–73 (2021).
- Simon R, Mukunda N. Twist phase in Gaussian-beam optics. *J Opt Soc Am A* 15, 2373–2382 (1998).
- Xu ZH, Liu XL, Chen YH et al. Self-healing properties of

Hermite-Gaussian correlated Schell-model beams. *Opt Express* **28**, 2828–2837 (2020).

43. Mandel L, Wolf E. *Optical Coherence and Quantum Optics* (Cambridge University Press, Cambridge, 1995).
44. Ma PJ, Kacerovská B, Khosravi R et al. Numerical approach for studying the evolution of the degrees of coherence of partially coherent beams propagation through an ABCD optical system. *Appl Sci* **9**, 2084 (2019).
45. Peng DM, Huang ZF, Liu YL et al. Optical coherence encryption with structured random light. *PhotonX* **2**, 6 (2021).
46. Zhang Z, Liu ZZ, Liu X et al. Measuring the orbital angular momentum of a vortex beam under extremely low coherence. *Appl Phys Lett* **122**, 011101 (2023).
47. Liu X, Chen Q, Zeng J et al. Measurement of optical coherence structures of random optical fields using generalized Arago spot experiment. *Opto-Electron Sci* **2**, 220024 (2023).
48. Wang F, Cai YJ. Experimental observation of fractional Fourier transform for a partially coherent optical beam with Gaussian statistics. *J Opt Soc Am A* **24**, 1937–1944 (2007).
49. Vallone G, D'Ambrosio V, Sponselli A et al. Free-space quantum key distribution by rotation-invariant twisted photons. *Phys Rev Lett* **113**, 060503 (2014).

Acknowledgements

We are grateful for National Key Research and Development Program of China (2022YFA1404800, 2019YFA0705000); National Natural Science Foundation of China (12104264, 12192254, 92250304, and 12374311); China Postdoctoral Science Foundation (2022T150392); Natural Science Foundation of Shandong Province (ZR2021QA014 and ZR2023YQ006); Qingchuang Science and Technology Plan of Shandong Province (2022KJ246).

Author contributions

The design and theoretical analysis were carried out by Z Zhang and GY Li, which was verified in experiment by Z Zhang, YL Liu, HY Wang and J Zeng; The writing—original draft by Z Zhang and J Zeng; The writing—review and editing was carried out by BJ Hoenders, CH Liang, YJ Cai and J Zeng. The entire research was supervised by CH Liang, YJ Cai and J Zeng; All authors have read and agreed to the published version of the manuscript.

Competing interests

The authors declare no competing financial interests.

Supplementary information

Supplementary information for this paper is available at <https://doi.org/10.29026/oes.2024.240001>



Scan for Article PDF